

Xia Ding

School of Aerospace Engineering,
Beijing Institute of Technology,
Beijing 100081, China;
Aerospace System Engineering Shanghai,
Shanghai 201109, China
e-mail: dingxia@bit.edu.cn

Yuchen Zhao

School of Aerospace Engineering,
Beijing Institute of Technology,
Beijing 100081, China
e-mail: yc.zhao@bit.edu.cn

Dong Yan

School of Aerospace Engineering,
Beijing Institute of Technology,
Beijing 100081, China
e-mail: yandong@bit.edu.cn

Kai Zhang¹

School of Aerospace Engineering,
Beijing Institute of Technology,
Beijing 100081, China
e-mail: zhangkai@bit.edu.cn

Controllable Propagation of Bending Waves in Wrinkled Films

Wrinkling is a common phenomenon in natural and engineering film structures. The wrinkles influence the geometry and dynamic response of these structures. In this work, we investigate the wrinkling of a stretched thin film containing engineered microstructures and its derived functionality on controlling the propagation of bending waves. The underlying mechanism is revealed and the effect of wrinkles on the bandgap of bending waves is systematically evaluated via numerical simulations based on the Bloch wave theory. We show that wrinkles with a customized wavelength can be triggered in the microstructured film due to the mismatched deformation in the film. The bandgap of the wrinkled film can be finely tuned via applied stretching, resulting in the controllable propagation of bending waves in thin films. Our work provides fundamental insights into wave propagation in wrinkled films and potential applications for dynamic control of the wave propagation in engineering film structures. [DOI: 10.1115/1.4043073]

1 Introduction

Thin-film structures are ubiquitous in nature and engineering [1–3], and their mechanical behaviors have received considerable attention, owing to the application of these structures in flexible electronics [4,5], material science [6,7], bioengineering [8,9], and aerospace engineering [2,10]. Wrinkling in a thin film is energetically favorable due to the negligible stiffness of the film experiencing compressive stresses [11–15]. Wrinkles usually change the structural geometry and lead to deviations in the corresponding mechanical behavior. Therefore, in traditional applications, wrinkling is regarded as a failure of the film structure and should be suppressed. However, in recent years, wrinkling has been harnessed for the design of new materials and structures [4,7,16–20]. Many studies have focused on generating controllable and ordered wrinkle patterns on free-standing thin films [21–23] or thin films on a substrate [17,24–26]. Moreover, the dynamic behavior of wrinkled film-substrate structures has received significant attention. Rudykh and Boyce [27] reported that wave propagation in highly deformable layered media can be controlled through elastic instability-induced wrinkling of interfacial layers. Li et al. [28] and Zheng et al. [29] investigated the wrinkling and propagation of elastic waves in a film-substrate bilayer system with surface/interfacial structures. A few studies have focused on the influence of wrinkles on the dynamic behavior of free-standing films [30], although free-standing nonuniform films have been widely used in engineering [10,31,32]. For example, free-standing nonuniform films are applied as a thin-film antenna in aerospace engineering, and the dynamic control of these films is a crucial issue in structural design.

Microstructures in a film can change the stress distribution as well as the wrinkle pattern [21–23]. Both the modal deformations for all the wave modes and bandgaps are compatible with the mechanical behavior of the lattice [33,34]. In this paper, we focus

on controllable wave propagation in free-standing microstructured thin films, obtained by introducing periodic strips and masses into a uniform film. We find that ordered wrinkles with a customized wavelength can be triggered by applied stretching, resulting in a switched bandgap of the microstructured film. The underlying mechanism governing the propagation of bending waves in the wrinkled film is revealed via numerical simulations based on the Bloch wave theory. Our work provides fundamental insights into wave propagation in wrinkled films as well as potential applications for dynamic control of the wave propagation in film structures.

This article is organized as follows. Section 2 describes a composite film composed of periodic microstructures designed with the aim of obtaining an ordered wrinkle pattern. The mechanism of film wrinkling is presented. Section 3 presents the results obtained from the investigation of band structures comprising the unwrinkled/wrinkled film with different tensile strains based on the Bloch wave theory. Section 4 presents the results of transient wave propagation analysis performed for verification of the predicted bandgaps. Section 5 details the findings describing the influence of the structural parameters on the bandgap structures.

2 Wrinkling of the Microstructured Thin Films

We introduce microstructures in a uniform thin film with the aim of generating an ordered wrinkle pattern. The influence of this pattern on the bending-wave propagation in the film is investigated. We also reveal the mechanism of wrinkling and determine the wavelength and amplitude of the wrinkles.

2.1 Design of the Microstructures. We design a microstructured thin film as shown in Fig. 1. The microstructures consist of periodic strips and masses, which share the same midsurface with the thin film. A side view of the film is shown in Fig. 2(a). Strips with a width of w_s are adhered on a uniform thin film, parallel and perpendicular to the applied stretching with a period of w . Square masses (side length: w_s) are located at the intersections of the strips. A polyimide thin film (density: 1.25 g/cm^3 , elastic modulus: 3 GPa , Poisson's ratio: 0.3 , and thickness t : 0.025 mm) is assumed. The strip is composed of the same material as the

¹Corresponding author.

Contributed by the Applied Mechanics Division of ASME for publication in the JOURNAL OF APPLIED MECHANICS. Manuscript received December 7, 2018; final manuscript received March 3, 2019; published online March 16, 2019. Assoc. Editor: Pedro Reis.

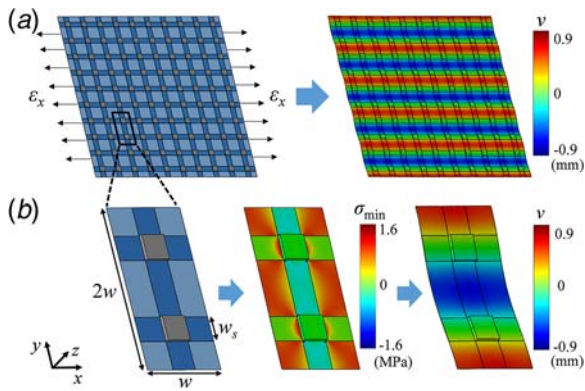


Fig. 1 (a) Schematic of the microstructured thin film (composed of 10×5 periodic unit cells) and the corresponding wrinkle pattern under a uniaxial stretching strain ϵ_x . The contour plot shows the out-of-plane displacement field v caused by wrinkles at $\epsilon_x = 3\epsilon_{cr}$. (b) Periodic unit cell and the distributions of minimum principal stresses σ_{min} before wrinkling ($\epsilon_x = 0.9\epsilon_{cr}$) and out-of-plane displacements v after wrinkling ($\epsilon_x = 3\epsilon_{cr}$). The corresponding dimensions of the film are $w = 20$ mm, $w_s = 6$ mm, and $t_s = 4t = 0.1$ mm.

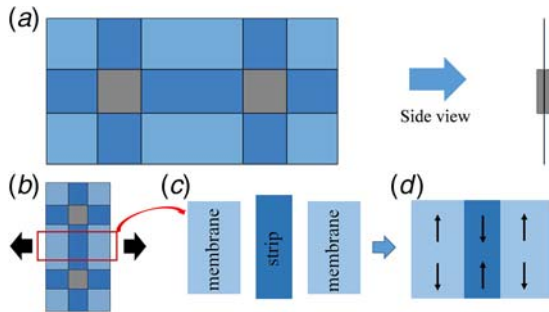


Fig. 2 (a) Side view and (b)–(d) the wrinkling mechanism of the microstructured thin film

film, but has a larger thickness t_s . The mass is fabricated from iron with a density, Poisson's ratio, thickness, and an elastic modulus of 7.8 g/cm^3 , 0.3 , 2 mm, and 200 GPa , respectively. Here, we consider the gravity effect by applying gravity field in the direction perpendicular to the plane. It is proved that the thin film is able to withstand the weight of the masses by calculating maximum principal stress and minimum principal stress in the film.

2.2 Wrinkling. We first consider the microstructured thin film shown in Fig. 1(a). The selection of a smallest unit cell depends on whether the film is wrinkled. The smallest unit cells of the flat film and the wrinkled film are a square region

(dimensions: $w \times w$) and a rectangular region (dimensions: $w \times 2w$), respectively, as shown in Fig. 1(b), $w = 20$ mm, $w_s = 6$ mm, and $t_s = 4t = 0.1$ mm. Numerical eigenvalue buckling and post-buckling analyses are both performed with the commercial finite element software ABAQUS. The buckling analysis is used to obtain the buckling modes and minimum eigenvalue. These modes are introduced as an imperfection into the postbuckling analysis, and the minimum eigenvalue is the critical buckling strain [35]. The thicknesses of strip, film, and mass mainly contribute to structural bending stiffness. Here, the whole film with microstructures is simplified as a 2D heterogeneous film in the finite element method. The film, strips, and masses are meshed by the shell element S4R with a linear elastic material model. The thicknesses of strip, film, and mass are assigned to the corresponding elements with 0.025 mm, 0.1 mm and 2 mm, respectively. Periodic boundary conditions are applied to each of the four edges. The top and bottom edges are free in the y -direction. The left and right edges are constrained in the x -direction by applying stretching corresponding to a maximum strain of 0.483% , i.e., $3\epsilon_{cr}$ ($\epsilon_{cr} = 0.161\%$ denotes the critical buckling strain of the film). In the post-buckling analysis, when the stretching strain exceeds the critical value ϵ_{cr} , periodic wrinkles parallel to the stretching direction occur in the thin film, as shown in Fig. 1(a). The half wavelength of the wrinkles is equal to the period of the strips, i.e., $\lambda/2 = w$. Figure 1(b) shows the minimum principal stress field in the unit cell (before wrinkling), subjected to a stretching strain of 0.145% ($0.9\epsilon_{cr}$). We can see that the compressive stresses, which trigger the wrinkling, are distributed in the strip.

To reveal the mechanism of the formed wrinkles, the stretching process is divided into two steps [22], as shown in Figs. 2(b)–2(d). First, we assume that the strip and the membrane are separated from each other, i.e., both are freely stretched in the x -direction, as shown in Fig. 2(c). The thickness of the strip is larger than that of the membrane. Hence, the stretch stress in the strip is smaller than that in the membrane. For equal Poisson's ratio values of the strip and the membrane, the strip shrinks less than the membrane in the y -direction. Second, the membrane and the strip are combined (see Fig. 2(d)), and during this process, the strip is compressed and the membrane is stretched in the direction perpendicular to the loading. The consequent internal compressive stresses generated in the strips trigger the buckling of the strips, i.e., the wrinkling phenomenon of the microstructured film.

2.3 Geometry of the Wrinkles. To customize the wrinkle pattern, we investigate the effect of microstructure on the wrinkle geometry. Focusing on the microstructural dimensions, we vary the width of the strips w_s , period of the strips w , and strip thickness to film thickness ratio t_s/t from 4 mm to 8 mm, 18 mm to 22 mm, and 3 to 5 , respectively. We perform postbuckling analysis on these thin films using finite element method (FEM) and determine the wavelength and amplitude of the wrinkles with increasing stretching strain. The half wavelength of the wrinkles is always equal to the period of the strips, i.e., $\lambda/2 = w$. As shown in Fig. 3, the amplitude increases with increasing stretching strain for all

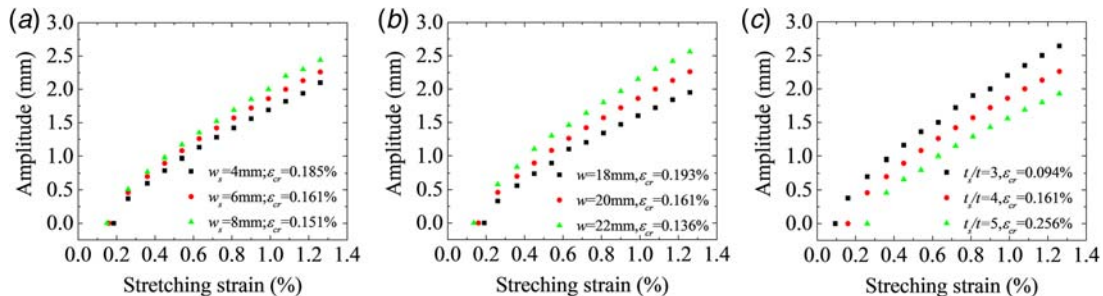


Fig. 3 Dependence of the wrinkle amplitude on the applied stretching strain associated with different (a) width of strips w_s , (b) period of strips w , and (c) strip thickness to film thickness ratio t_s/t

cases. However, for a given strain level, the wrinkle amplitude of a film with wider, sparser, or thinner strips is, in general, larger than that of a film with narrower, denser, or thicker strips. The results also reveal that the wavelength of the wrinkles can only be changed by modifying the period of the strips, whereas the amplitude can be dynamically and independently tuned by adjusting the applied stretching.

3 Bandgap Structures of the Wrinkled Thin Film at Different Stretching Strains

3.1 Bloch Wave Analysis. We use energy-band theory to investigate the propagation of bending waves in a thin film (Fig. 4). The periodic unit cell and the corresponding irreducible Brillouin zone for the wrinkled films and the flat films are shown in Figs. 4(f) and 4(g), respectively. Stretching the unit cell under periodic boundary conditions, the deformation and stresses at different stretching strains are extracted and then input into a same model to execute the frequency analysis in ABAQUS. According to the Bloch wave theory, elastic waves propagating in a periodic structure can be expressed as

$$\mathbf{U}(\mathbf{R}, t) = \Phi(\mathbf{R})e^{i(\mathbf{K}\cdot\mathbf{R}-\omega t)} \quad (1)$$

where $\Phi(\mathbf{R})$ is a periodic function with the same periodicity as the structure and $\mathbf{U}(\mathbf{R}, t)$ is the dynamic displacement, which is a function of the position coordinates \mathbf{R} and the time t . ω and \mathbf{K} are the angular frequency and wave vector, respectively. Therefore,

$$\mathbf{U}(\mathbf{R}_n + \mathbf{R}) = \mathbf{U}(\mathbf{R})e^{i\mathbf{K}\cdot\mathbf{R}_n} \quad (2)$$

where \mathbf{R}_n is a lattice vector.

The dispersion relation of a periodic structure can be solved by commercial finite element codes with Bloch-type boundary conditions [29,36]. Arraying the wrinkled unit cell into two models, the displacement $\mathbf{U}(\mathbf{R})$ can be described via the complex expression $\mathbf{U}(\mathbf{R}) = \mathbf{U}_{\text{Re}} + i\mathbf{U}_{\text{Im}}$, where the subscripts Re and Im denote the real and imaginary parts of $\mathbf{U}(\mathbf{R})$, respectively. For our proposed

thin film, we define

$$\mathbf{U}_{\text{Re}}^r = \mathbf{U}_{\text{Re}}^l \cos(kw) - \mathbf{U}_{\text{Im}}^l \sin(kw)$$

$$\mathbf{U}_{\text{Im}}^r = \mathbf{U}_{\text{Re}}^l \sin(kw) + \mathbf{U}_{\text{Im}}^l \cos(kw)$$

$$\mathbf{U}_{\text{Re}}^u = \mathbf{U}_{\text{Re}}^b \cos(2kw) - \mathbf{U}_{\text{Im}}^b \sin(2kw)$$

$$\mathbf{U}_{\text{Im}}^u = \mathbf{U}_{\text{Re}}^b \sin(2kw) + \mathbf{U}_{\text{Im}}^b \cos(2kw)$$

where the superscripts r , l , u , and b denote the right, left, upper, and lower boundary, respectively. k is the wave number. w and $2w$ denote the projections of lattice vectors on the x -axis and y -axis, respectively. To implement Bloch-type boundary conditions in ABAQUS, we add Eq. (3) to our FEM model through equation constraints contained in ABAQUS. The corresponding circular frequency, which yields the band structure of the thin film, is determined via natural frequency analysis of each wave vector associated with the irreducible Brillouin zone.

3.2 Evolution of the Bandgap Structures. We determine the dispersion relation of the thin film (see Figs. 4(a)–4(e)) at stretching strains of $0\epsilon_{cr}$, $0.5\epsilon_{cr}$, $1\epsilon_{cr}$, $1.5\epsilon_{cr}$, and $3\epsilon_{cr}$. The band structures indicate that a bandgap of bending waves forms prior to wrinkling. When the stretching strain surpasses ϵ_{cr} , the bandgap perpendicular to the direction of wrinkling is closed, while a directional bandgap along the wrinkles remains until the strain reaches $3\epsilon_{cr}$. Subsequently, the entire bandgap closes and transforms to a passband.

Figure 5 shows the band structures calculated for the unstretched film with and without localized masses. The five modes occurring at the representative frequency locations are presented in each configuration. Similar mode shapes occur at the corresponding positions of the two band structures, where the vibration of the mass is not dominant. When the masses are added to the film, bandgaps occur. We also investigate the effect of density of the mass on the bandgap of the unstretched film. The bandgaps widen with increasing density of the masses. However, the formed bandgap is not due to locally resonant effect. The reason can be explained from three points of view. First, the local mass is directly attached to the

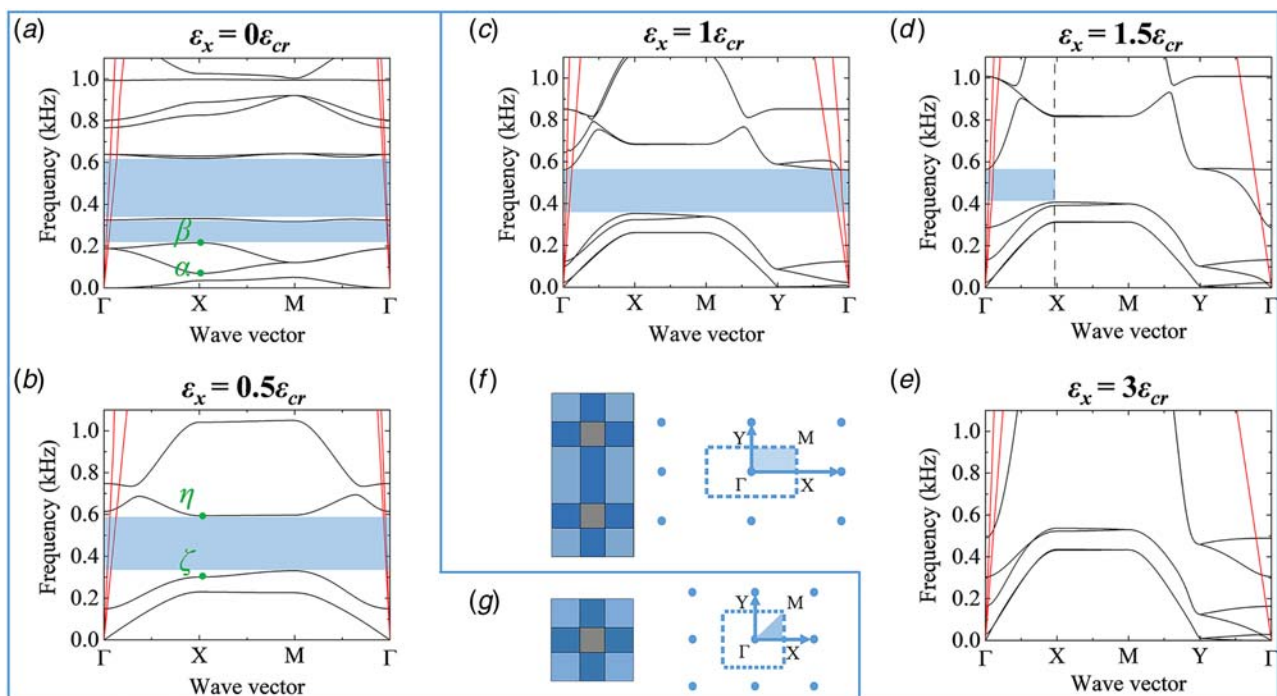


Fig. 4 Bandgap structures at the stretching strain of (a) $0\epsilon_{cr}$, (b) $0.5\epsilon_{cr}$, (c) $1\epsilon_{cr}$, (d) $1.5\epsilon_{cr}$, and (e) $3\epsilon_{cr}$. (f) and (g) The unit cell and corresponding irreducible Brillouin zone of the wrinkled film and the flat film, respectively.

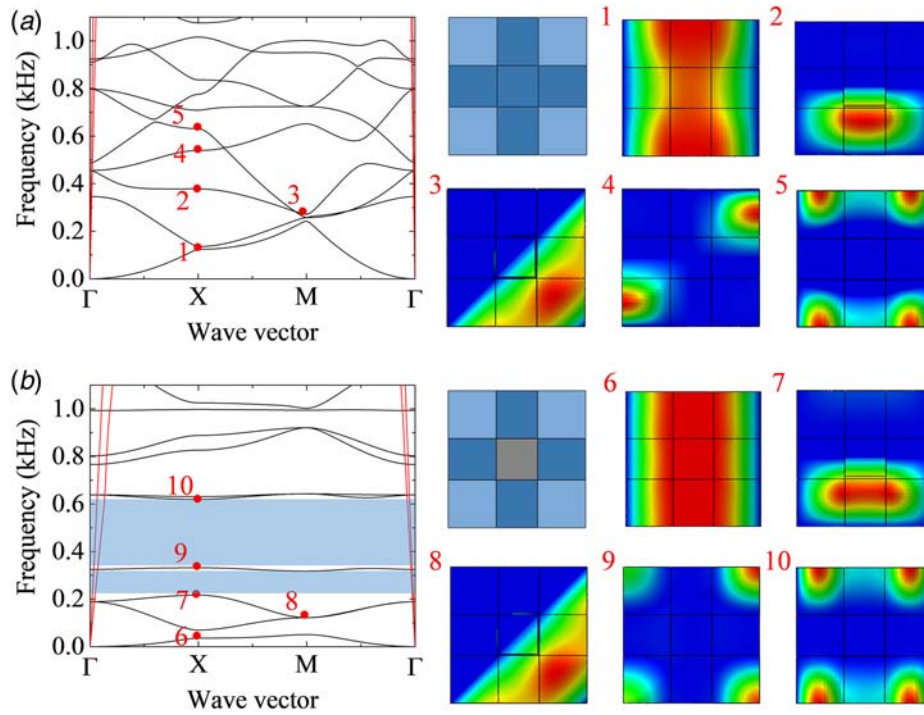


Fig. 5 Band structures of the unstretched film without mass (a) and with mass (b), and the corresponding five modes

film without rubber layer between them. Thus, there is no local resonator in the film, although local mass is introduced. Second, the mode shape, located at the lower boundary of the bandgap (mode 7), does not exhibit the characteristic of locally resonant mode, where the local mass is vibrating while the substrate is at rest. In addition, the bandgap profile does not satisfy the feature of a typical local resonance bandgap profile, where the lower mode flattens at the edge of the irreducible Brillouin zone, while the first mode above the bandgap has a minimum when the wave number is equal to 0. The local mass, therefore, changes the

impedance mismatch between different regions of the films and alters the bandgaps based on Bragg-scattering mechanisms.

When the structure is stretched, the effective stiffness of the stretched film increases, making the calculated Eigen frequencies increase. In Figs. 6(a)–6(d), we extract the modes in the second and third branches at strain $0\epsilon_{cr}$, $0.05\epsilon_{cr}$, $0.1\epsilon_{cr}$, and $0.5\epsilon_{cr}$, respectively. We find that, under a small extension (e.g., $0.05\epsilon_{cr}$), the mode shape of the second branch at X point (mode γ) is different from mode α at $0\epsilon_{cr}$, while that of the third branch is the same as mode β at $0\epsilon_{cr}$. As shown in Fig. 6(c), the second branch has

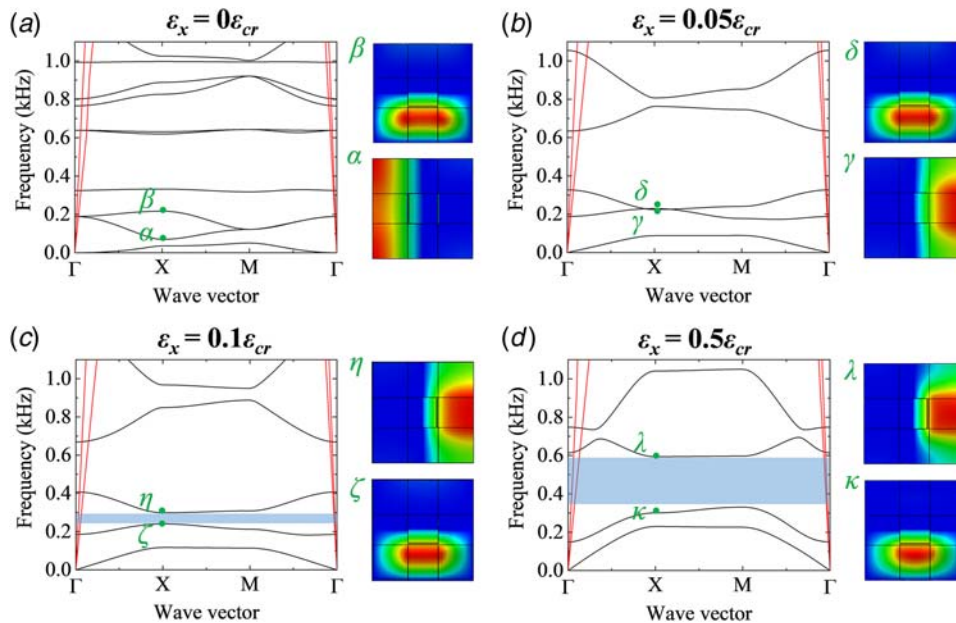


Fig. 6 The modes in the second and third branches at strain (a) $0\epsilon_{cr}$, (b) $0.05\epsilon_{cr}$, (c) $0.1\epsilon_{cr}$, and (d) $0.5\epsilon_{cr}$

become the third branch over strain $0.05\epsilon_{cr}$. As the increasing of stretching strain along x -direction, the third branch (mode η) for the stretched film rises faster than the second branch (mode ζ), as shown in Figs. 6(c) and 6(d). Under the stretching, a bandgap between the second and third modes is triggered.

When the stretching strain is beyond ϵ_{cr} , in contrast to that of the flat thin film, a longitudinal vibration mode perpendicular to the direction of wrinkling is missing from Fig. 7(a). This indicates that the coupling of longitudinal waves and bending waves results in bandgap closure along this direction. To understand this closure, we remove the internal stresses, but maintain a thin-film deformation level of $1.2\epsilon_{cr}$ and perform frequency analysis on the film by sweeping the irreducible Brillouin zone. The dispersion relation in Fig. 7(b) reveals similar coupling features of longitudinal waves and bending waves. This confirms that the bandgap closure perpendicular to the direction of wrinkling results mainly from the bending deformation of wrinkling, rather than the internal stresses, at a given strain level.

In Fig. 7(c), we plot the frequency of mode θ and mode τ as a function of increasing ϵ_x/ϵ_{cr} after buckling. The frequency of mode θ decreases with increasing stretching strain, whereas the frequency of mode τ increases. When the stretching strain reaches $2.6\epsilon_{cr}$, the two curves intersect and close the bandgap in the direction of wrinkling. We calculate the bandgap structure when the stretching strain is $2.8\epsilon_{cr}$, where bandgap closure occurs along the wrinkles, as shown in Fig. 7(d). We can see that the gap in Fig. 7(e) remains open if we maintain a thin-film deformation of $2.8\epsilon_{cr}$ and ignore the internal stresses. The results indicate that the closed bandgap along the wrinkle direction results from the increasing internal stresses, rather than the deformation of the wrinkled film.

4 Propagation of Bending Waves in Microstructured Thin Films

To demonstrate the feasibility of thin-film tuning the bandgap through manipulation of the film wrinkle, we investigate the

dynamic response of thin films via FEM simulation of the bending-wave propagation. In our transient analyses, a small linear perturbation is applied to a heavily deformed film. Two models are considered here: a supercell with periodic boundary conditions and a finite film structure with two clamped ends. For the former, as shown in Fig. 8(a), the supercell is composed of 10×5 unit cells with the same geometric and material parameters as the unit cell shown in Fig. 1(b). For the latter, a finite thin film consisting of 60×5 unit cells is modeled with two clamped ends, as shown in Fig. 9(a).

4.1 Dynamic Simulations. We investigate the dynamic response of the thin film by simulating the propagation of bending waves using ABAQUS. The supercell is meshed by the shell element S4R with a linear elastic material model. Periodic boundary conditions are applied to each of the edges. The film is stretched by a maximum strain of 0.483% ($3\epsilon_{cr}$) in the x -direction. Afterward, we use the restart analysis in ABAQUS Standard to extract the deformation and stresses of the thin film at stretching strains of $0.5\epsilon_{cr}$, $1.5\epsilon_{cr}$, and $3\epsilon_{cr}$. These are then assigned to the same model (in ABAQUS Explicit). For the model of the wrinkled film, periodic boundary conditions are applied to the top and bottom of the film, and the horizontal displacement is constrained on the left and right edges. An out-of-plane harmonic excitation with an amplitude of 0.01 mm at 450 Hz is then exerted at the left edge. The propagation of bending waves along the direction of the wrinkling is determined via the transient analysis of the film. Similarly, the propagation of bending waves perpendicular to this direction is simulated. Here, periodic boundary conditions are applied to the left and right edges, and an out-of-plane harmonic excitation with the aforementioned amplitude and frequency is exerted at the bottom edge.

We further demonstrate the feasibility of the proposed method by considering a finite thin film with two clamped ends, rather than periodic boundary conditions, as shown in Fig. 9(a). At 450 Hz, an out-of-plane excitation with an amplitude of 0.01 mm is exerted at the center of the film under stretching strains of $0.5\epsilon_{cr}$, $1.5\epsilon_{cr}$, and $3\epsilon_{cr}$.

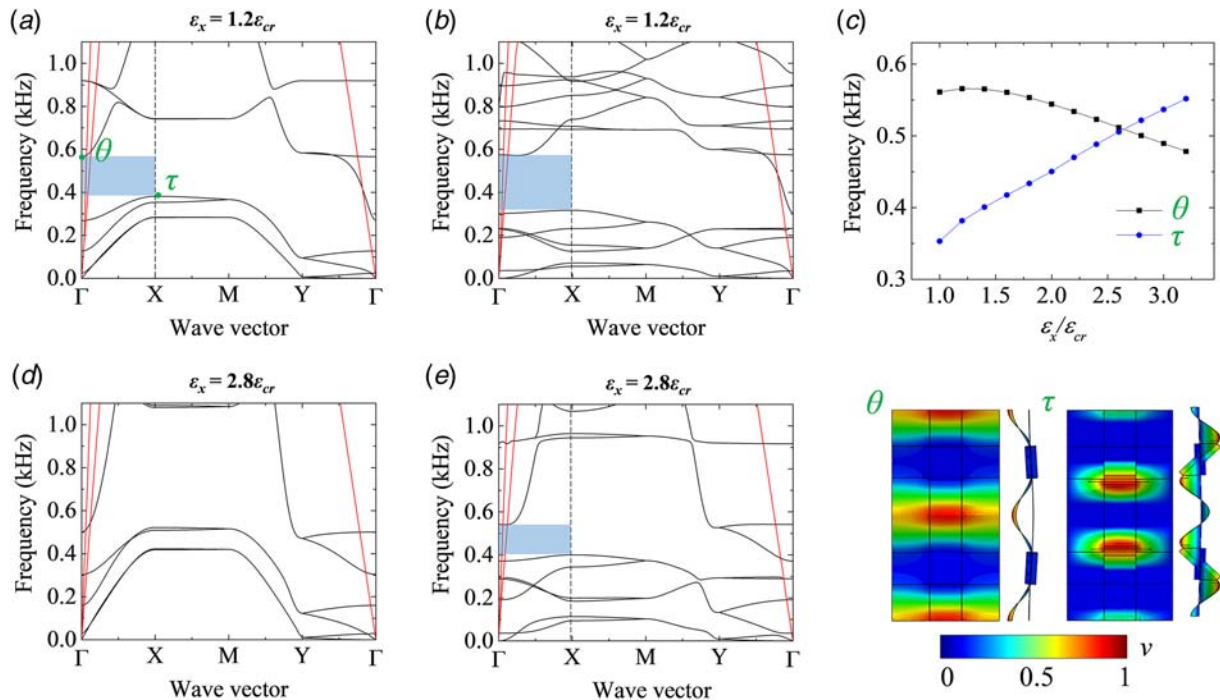


Fig. 7 Bandgap structures at the stretching strain of (a) and (b) $1.2\epsilon_{cr}$, (d) and (e) $2.8\epsilon_{cr}$. In (b) and (e), internal stresses in the wrinkled thin film are removed and only the deformation is considered. (c) Frequency dependence of deformation mode θ and mode τ on increasing ϵ_x/ϵ_{cr} after buckling.

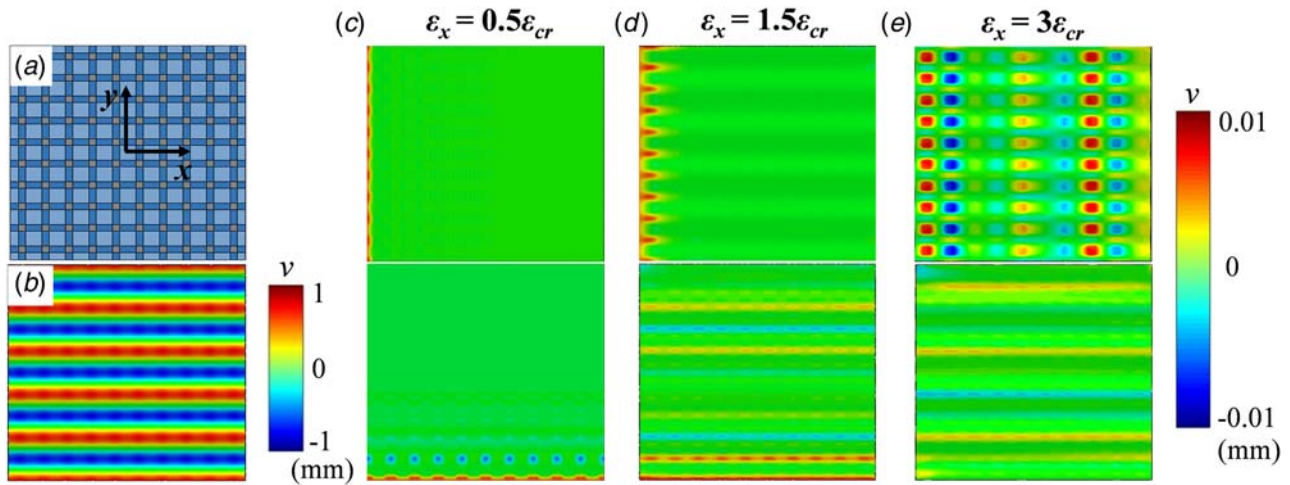


Fig. 8 (a) Supercell consisting of 10×5 unit cells with periodic boundary conditions and (b) the corresponding wrinkle pattern at stretching strain $3\epsilon_{cr}$. The out-of-plane displacement fields of the thin film under a 450 Hz harmonic excitation with an amplitude of 0.01 mm exerted at the left or bottom edge, when the stretching strain is (c) $0.5\epsilon_{cr}$, (d) $1.5\epsilon_{cr}$, and (e) $3\epsilon_{cr}$.

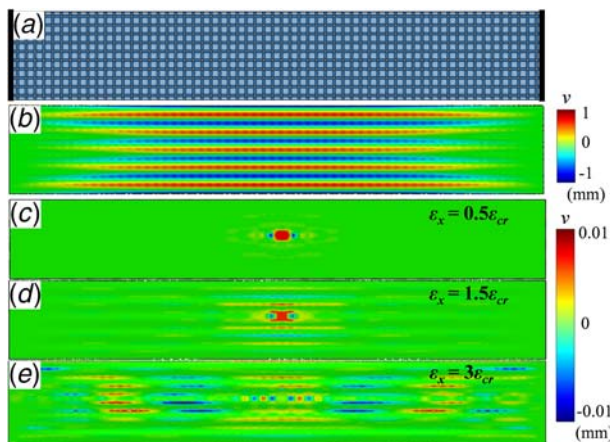


Fig. 9 (a) Finite thin film consisting of 60×5 unit cells with two clamped ends and (b) the corresponding wrinkle pattern at stretching strain $3\epsilon_{cr}$. The out-of-plane displacement fields of the thin film under a 450 Hz harmonic excitation with an amplitude of 0.01 mm exerted at the center, when the stretching strain is (c) $0.5\epsilon_{cr}$, (d) $1.5\epsilon_{cr}$, and (e) $3\epsilon_{cr}$.

4.2 Propagation of Bending Waves in Both Directions.

When the stretching strain of the film surpasses the critical buckling strain, parallel wrinkles form along the stretching direction with a half wavelength equal to the period of the strips. This result is obtained for both models (see Figs. 8(b) and 9(b)), except for the regions close to the clamped ends of the finite thin film. At a stretching strain of $0.5\epsilon_{cr}$, bending waves can not propagate in both directions (Figs. 8(c) and 9(c)), since the frequency of 450 Hz is located in the bandgap (Fig. 4(b)). At $1.5\epsilon_{cr}$, waves can only propagate in the direction perpendicular to the wrinkles (Figs. 8(d) and 9(d)), since the bandgap becomes directional. Waves can propagate in both directions as the bandgap switches to a passband over $3\epsilon_{cr}$ (Fig. 4(e)). These results indicate that, by controlling the applied stretching, we can dynamically switch the opening and closing of the bandgap. The results from the transient analysis of the finite thin film correspond closely to the results obtained via the Bloch wave analysis. Furthermore, the results demonstrate the capability of our method to dynamically control the propagation of bending waves in a thin film with a finite size and subjected to realistic boundary conditions.

5 Parametric Study

To understand the bending-wave propagation in wrinkled films and guide the design of microstructures in engineering film structures for controlling the wave propagation, we systematically investigate the effect of microstructures on the bandgap. During this parametric study, the period, thickness, and width of the strips (w , t_s/t , and w_s , respectively) as well as the density of masses ρ are varied. We will show that the wrinkles and bandgap can be tailored by designing the proposed microstructures.

5.1 Period of Strips. We vary the period of the strips w from 17 mm to 23 mm and determine the gap range and lower frequency at different stretching strains, as shown in Figs. 10(a) and 10(b). Changes in the gap range of the flat film differ from those of the wrinkled film. The gap range is almost constant with increasing w before the film wrinkles, but decreases after wrinkling. When the curve intersects the x -axis, the gap is closed. Furthermore, the lower frequency of the gap always decreases with increasing w (Fig. 10(b)). The dashed line indicates the envelope of lower frequency during stretching. We also obtain the threshold of the stretching strain for closing of the gap against the period of the strips, which decreases monotonously, as shown in Fig. 10(c). The results show that, compared with denser films, a thin film with sparser strips can have a bandgap with a lower frequency, but a smaller range at a given strain level; the switchable gap can be realized at a smaller loading level, which is favorable for engineering film structures. Therefore, the gap range, lower frequency, and threshold of the stretching strain for the closed gap can be tuned by varying the period of the strips.

5.2 Thickness of Strips. Subsequently, we vary the strip thickness to film thickness ratio t_s/t from 2 to 5. The evolution of the gap range and lower frequency associated with different stretching strains are shown in Figs. 11(a) and 11(b). The frequency increases with increasing t_s/t but changes in the gap range before and after wrinkling are described by different trends. Before wrinkling, the gap range increases rapidly and monotonously with increasing t_s/t , but the rate of increase decreases gradually after wrinkling. The gap range decreases when the strip is relatively thick. Figure 11(c) indicates that, compared with those characterized by smaller differences, the film with a larger difference in the film and strip thicknesses has a lower threshold strain when the gap is closed. Furthermore, this strain decreases almost linearly

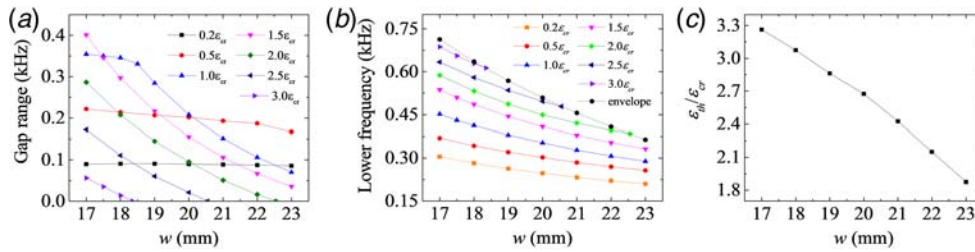


Fig. 10 (a) Gap range, (b) lower frequency of the bandgap, and (c) normalized threshold of the stretching strain for a closed gap with different period of the strips

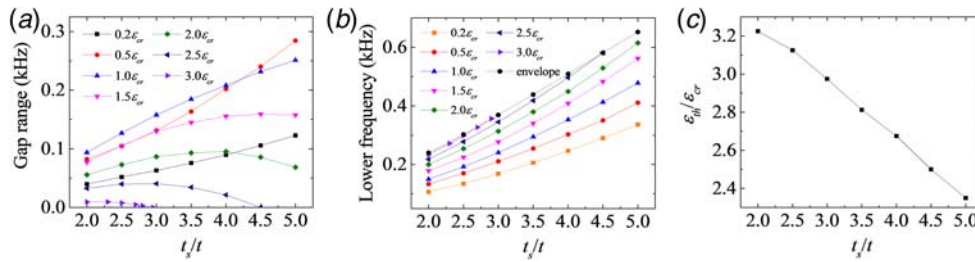


Fig. 11 (a) Gap range, (b) lower frequency of the bandgap, and (c) normalized threshold of the stretching strain for the closed gap with different thickness of strips

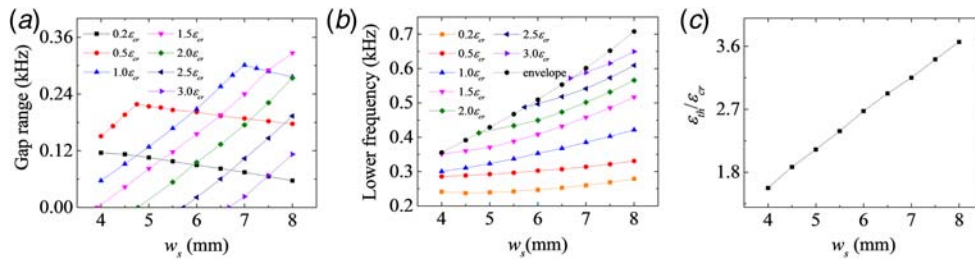


Fig. 12 (a) Gap range, (b) lower frequency of the bandgap, and (c) normalized threshold of the stretching strain for the closed gap with different width of strips

with increasing t_s/t . These results indicate that we can also tune the bandgap by varying the thickness ratio t_s/t .

5.3 Width of Strips. We further study the effect of strip width w_s on the bandgap by varying w_s from 4 mm to 8 mm, as shown in Fig. 12. When w_s increases, the gap range of the nonwrinkled films decreases, whereas the gap range of the wrinkled film increases. The lower frequency and the threshold of stretching strain always increase with increasing w_s (Figs. 12(a) and 12(b)). For a given strain level beyond wrinkling, the thin film with wider strips can experience a higher frequency and control a

wider range of bending waves than films with narrower strips; the bandgap closes at a relatively higher stretching level.

5.4 Density of Masses. Finally, we investigate the effect of masses on the propagation of bending waves under stretching. The density of masses ρ varied from 2.7 g/cm³ to 12 g/cm³, and the corresponding changes in the features of the bandgap are noted (see Fig. 13). As for the unstretched film, the bandgaps broaden with increasing ρ (Sec. 3.2), in contrast to the evolution of the stretching film gap range. As ρ increases, the bandgaps decrease before wrinkling, but increase after wrinkling (Fig. 13(a)).

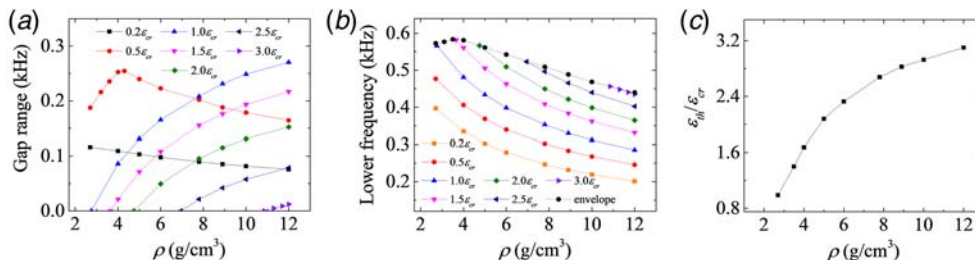


Fig. 13 (a) Gap range, (b) lower frequency of the bandgap, and (c) normalized threshold of the stretching strain for the closed gap with different density of masses

The evolution of the gap range associated with the lower frequency evolves in the opposite manner, i.e., the frequency decreases with increasing ρ (Fig. 13(b)). Moreover, the threshold of the stretching strain increases significantly with increasing ρ (Fig. 13(c)).

6 Conclusion

In this work, we study the propagation of bending waves in wrinkled thin films and propose dynamic control of the wave propagation in the film structure via manipulation of the film wrinkle. We design a microstructured thin film with periodic strips and masses to achieve the customized wrinkle pattern. The mismatched deformation between the film and the strips in each unit cell results in the formation of wrinkles. The half wavelength of these wrinkles is equal to the period of the strips, whereas the amplitude depends on the applied stretching. Owing to the coupling of bending waves and longitudinal waves, adjustment of the applied stretching that triggers the wrinkling leads to closure of the bandgap in the direction perpendicular to the wrinkles. However, the bandgap in the direction parallel to the wrinkles can be closed with increasing stresses. We can control the propagation of bending waves in a wrinkled thin film via the applied stretching and precisely adjust the frequency range and lower frequency of the bandgap through microstructural design. An understanding of bending-wave propagation in wrinkled thin films can guide us in microstructural design aimed at controlling the wave propagation. Most of the films used in engineering applications are nonuniform. For example, in aerospace film antenna, electrical components are adhered on the film in order to achieve specific functionalities. These components can be further designed and used as microstructures for generating desired wrinkle patterns. Our investigation also provides an avenue for using the intrinsic wrinkles in a structure to suppress the propagation of vibrations. The simple wave control strategy of the proposed method has potential applications in practical engineering film structures.

Acknowledgment

We thank Jianlong Chen for assistance with the numerical simulations. Financial support from the National Science Foundation of China (Nos. 11672037 and 11290153) and Key Laboratory in Aerospace System Engineering Shanghai is also acknowledged.

References

- [1] Savin, T., Kurpios, N. A., Shyer, A. E., Florescu, P., Liang, H., Mahadevan, L., and Tabin, C. J., 2011, "On the Growth and Form of the Gut," *Nature*, **476**(7358), pp. 57–62.
- [2] Wong, Y. W., and Pellegrino, S., 2006, "Wrinkled Membranes Part I: Experiments," *J. Mech. Mater. Struct.*, **1**(1), pp. 3–25.
- [3] Li, B., Cao, Y.-P., Feng, X.-Q., and Gao, H., 2012, "Mechanics of Morphological Instabilities and Surface Wrinkling in Soft Materials: A Review," *Soft Matter*, **8**(21), pp. 5728–5745.
- [4] Rogers, J. A., Someya, T., and Huang, Y., 2010, "Materials and Mechanics for Stretchable Electronics," *Science*, **327**(5973), pp. 1603–1607.
- [5] Singamaneni, S., and Tsukruk, V. V., 2010, "Buckling Instabilities in Periodic Composite Polymeric Materials," *Soft Matter*, **6**(22), pp. 5681–5692.
- [6] Croll, A. B., and Crosby, A. J., 2012, "Pattern Driven Stress Localization in Thin Diblock Copolymer Films," *Macromolecules*, **45**(9), pp. 4001–4006.
- [7] Harris, J. M., Huh, J. Y., Semler, M. R., Ihle, T., Stafford, C. M., Hudson, S. D., Fagan, J. A., and Hobbie, E. K., 2013, "Elasticity and Rigidity Percolation in Flexible Carbon Nanotube Films on PDMS Substrates," *Soft Matter*, **9**(48), pp. 11568–11575.
- [8] Cerda, E., and Mahadevan, L., 2003, "Geometry and Physics of Wrinkling," *Phys. Rev. Lett.*, **90**(7), p. 074302.
- [9] Massabò, R., and Gambarotta, L., 2007, "Wrinkling of Plane Isotropic Biological Membranes," *ASME J. Appl. Mech.*, **74**(3), pp. 550–559.
- [10] Johnson, L., Young, R., Montgomery, E., and Alhorn, D., 2011, "Status of Solar Sail Technology Within NASA," *Adv. Space Res.*, **48**(11), pp. 1687–1694.
- [11] Wong, Y. W., and Pellegrino, S., 2006, "Wrinkled Membranes Part II: Analytical Models," *J. Mech. Mater. Struct.*, **1**(1), pp. 27–61.
- [12] Lin, S., Mao, Y., Radovitzky, R., and Zhao, X., 2017, "Instabilities in Confined Elastic Layers Under Tension: Fringe, Fingering and Cavitation," *J. Mech. Phys. Solids*, **106**, pp. 229–256.
- [13] Cerda, E., Ravi-Chandar, K., and Mahadevan, L., 2002, "Wrinkling of an Elastic Sheet Under Tension," *Nature*, **419**(6907), pp. 579–580.
- [14] Nayyar, V., Ravi-Chandar, K., and Huang, R., 2011, "Stretch-Induced Stress Patterns and Wrinkles in Hyperelastic Thin Sheets," *Int. J. Solids Struct.*, **48**(25–26), pp. 3471–3483.
- [15] Wang, B., Ghanta, P., Vinnikova, S., Bao, S., Liang, J., Lu, H., and Wang, S., 2017, "Wrinkling of Tympanic Membrane Under Unbalanced Pressure," *ASME J. Appl. Mech.*, **84**(4), p. 041002.
- [16] Kim, T. H., Choi, W. M., Kim, D. H., Meitl, M. A., Menard, E., Jiang, H., Carlisle, J. A., and Rogers, J. A., 2008, "Printable, Flexible, and Stretchable Forms of Ultrananocrystalline Diamond With Applications in Thermal Management," *Adv. Mater.*, **20**(11), pp. 2171–2176.
- [17] Cao, Y.-P., Li, B., and Feng, X.-Q., 2012, "Surface Wrinkling and Folding of Core-Shell Soft Cylinders," *Soft Matter*, **8**(2), pp. 556–562.
- [18] Chan, H. F., Zhao, R., Parada, G. A., Meng, H., Leong, K. W., Griffith, L. G., and Zhao, X., 2018, "Folding Artificial Mucosa With Cell-Laden Hydrogels Guided by Mechanics Models," *Proc. Natl. Acad. Sci.*, **115**(29), pp. 7503–7508.
- [19] Terwagne, D., Brojan, M., and Reis, P. M., 2014, "Smart Morphable Surfaces for Aerodynamic Drag Control," *Adv. Mater.*, **26**(38), pp. 6608–6611.
- [20] Reis, P. M., 2015, "A Perspective on the Revival of Structural (In) Stability With Novel Opportunities for Function: From Buckliphobia to Buckliphilia," *ASME J. Appl. Mech.*, **82**(11), p. 111001.
- [21] Yan, D., Zhang, K., Peng, F., and Hu, G., 2014, "Tailoring the Wrinkle Pattern of a Microstructured Membrane," *Appl. Phys. Lett.*, **105**(7), p. 071905.
- [22] Yan, D., Zhang, K., and Hu, G., 2016, "Wrinkling of Structured Thin Films Via Contrasted Materials," *Soft Matter*, **12**(17), pp. 3937–3942.
- [23] Yan, D., Huangfu, D., Zhang, K., and Hu, G., 2016, "Wrinkling of the Membrane With Square Rigid Elements," *EPL*, **116**(2), p. 24005.
- [24] Bowden, N., Brittain, S., Evans, A. G., Hutchinson, J. W., and Whitesides, G. M., 1998, "Spontaneous Formation of Ordered Structures in Thin Films of Metals Supported on an Elastomeric Polymer," *Nature*, **393**(6681), pp. 146–149.
- [25] Huang, Z. Y., Hong, W., and Suo, Z., 2005, "Nonlinear Analyses of Wrinkles in a Film Bonded to a Compliant Substrate," *J. Mech. Phys. Solids*, **53**(9), pp. 2101–2118.
- [26] Huang, R., and Im, S. H., 2006, "Dynamics of Wrinkle Growth and Coarsening in Stressed Thin Films," *Phys. Rev. E*, **74**(2), p. 026214.
- [27] Rudykh, S., and Boyce, M. C., 2014, "Transforming Wave Propagation in Layered Media Via Instability-Induced Interfacial Wrinkling," *Phys. Rev. Lett.*, **112**(3), p. 034301.
- [28] Li, G.-Y., Zheng, Y., Cao, Y., Feng, X.-Q., and Zhang, W., 2016, "Controlling Elastic Wave Propagation in a Soft Bilayer System Via Wrinkling-Induced Stress Patterns," *Soft Matter*, **12**(18), pp. 4204–4213.
- [29] Zheng, Y., Li, G.-Y., Cao, Y., and Feng, X.-Q., 2017, "Wrinkling of a Stiff Film Resting on a Fiber-Filled Soft Substrate and Its Potential Application as Tunable Metamaterials," *Extreme Mech. Lett.*, **11**, pp. 121–127.
- [30] Hossain, N. M. A., Jenkins, C. H., Woo, K., and Igawa, H., 2006, "Transverse Vibration Analysis for Partly Wrinkled Membranes," *J. Spacecr. Rockets*, **43**(3), pp. 626–637.
- [31] Luo, Y., Xing, J., Niu, Y., Li, M., and Kang, Z., 2017, "Wrinkle-Free Design of Thin Membrane Structures Using Stress-Based Topology Optimization," *J. Mech. Phys. Solids*, **102**, pp. 277–293.
- [32] Freeland, R. E., Bilyeu, G. D., Veal, G. R., Steiner, M. D., and Carson, D. E., 1997, "Large Inflatable Deployable Antenna Flight Experiment Results," *Acta Astronaut.*, **41**(4–10), pp. 267–277.
- [33] Scarpa, F., Ouisse, M., Collet, M., and Saito, K., 2013, "Kirigami Auxetic Pyramidal Core: Mechanical Properties and Wave Propagation Analysis in Damped Lattice," *ASME J. Vib. Acoust.*, **135**(4), p. 041001.
- [34] Ouisse, M., Collet, M., and Scarpa, F., 2016, "A Piezo-Shunted Kirigami Auxetic Lattice for Adaptive Elastic Wave Filtering," *Smart Mater. Struct.*, **25**(11), pp. 115016.
- [35] Wong, Y. W., and Pellegrino, S., 2006, "Wrinkled Membranes Part III: Numerical Simulations," *J. Mech. Mater. Struct.*, **1**(1), pp. 63–95.
- [36] Åberg, M., and Gudmundson, P., 1997, "The Usage of Standard Finite Element Codes for Computation of Dispersion Relations in Materials With Periodic Microstructure," *J. Acoust. Soc. Am.*, **102**(4), pp. 2007–2013.